NUCLEATE BOILING IN SQUARE ARRAYS OF SUBCOOLED WATER SPRAYS

Ricardo Hernandez Pereira, ricardo.pereira@mecanica.ufu.br
Enio Pedone Bandarra Filho, bandarra@mecanica.ufu.br
Faculty of Mechanical Engineering – Federal University of Uberlandia, Av. Joao Naves de Avila, 2121 – Uberlandia-MG-Brazil.

Sérgio Leal Braga, slbraga@puc-rio.br
José Alberto dos Reis Parise, parise@puc-rio.br
Pontifícia Universidade Católica do Rio de Janeiro, Rua Marquês de São Vicente 225, Gávea - Rio de Janeiro, RJ, Brazil.

Abstract. The nucleate boiling of highly subcooled water, under 100 cm^2 square arrays of impinging sprays, was experimentally investigated. Three types of commercially-available full cone pressure nozzles, of distinct flow capabilities, allowed for runs where the average impinging coolant mass flux spanned the 0.3 – 7.2 kg/m^{2}s range. Array geometry was varied adjusting nozzle-to-nozzle and nozzle-to-impingement surface distances. Experimental construction allowed for good drainage of spent coolant and unrestricted air entrainment to spray cones. The average heat flux through the heated, upward-facing, copper impingement surface was found to be equal to the sum of single-phase, q"$_{SP}$, and nucleate boiling, q"$_{NB}$, heat flux components. The phase change component, experimentally observed to depend upon wall excess temperature only, was correlated by $q"_{NB}=2067(T_W-T_{SAT})^{1.57}$. The $q"_{SP}+q"_{NB}$ expression reproduces all the 149 original experimental points with a mean absolute error of 10.6 %. Non-CHF cooling effectiveness and efficiencies of up to, respectively, 2,000 kJ/kg and 83 % were observed.

Keywords: Nucleate Boiling, Square arrays, Subcooled, Water, Sprays.

1. INTRODUCTION

Attention has been given, over the years, to spray impingement boiling. Multiple droplet impact, over a heat-dissipating surface, leads to enhanced heat transfer on all nucleate, transition and film boiling regimes. Increased critical (maximum) heat flux is also often associated to spray impingement. The technique has been traditionally employed for the controlled quenching of steel and non-ferrous parts [1,2]. More recently, spray impingement of dielectric fluids has been considered for the evaporative cooling of novel electronic components [3-5]. The continued miniaturization of microprocessors keeps posing new challenges to their thermal management. Heat fluxes of present day components, to be dissipated over moderate component-to-coolant temperature differences, call for advanced phase change convective schemes. Rybicki and Mudawar [3] refer to much of the earlier literature-available data and heat transfer correlations.

Information on multiple, overlapping or not, spray nozzles arrangements is scarce [2,4-9]. As in the case of jet arrays, multiple spray nozzles must be positioned in some repetitive pattern if impingement flow heat transfer enhancement is to be extended to the processing of large surface products. The understanding of phenomena involved in jet impingement boiling, specially referring to the fully developed nucleate boiling regime, may be considered to be, today, comparatively mature [10]. Much knowledge was accumulated on jet impingement hydrodynamics, single-phase forced convection, boiling incipience and onset, fully developed nucleate boiling, critical heat flux, transition and film boiling regimes. System-specific effects on those topics, such as: a) surface finish and enhancements (fins), b) jet geometry and velocity, c) fluid properties and interaction with impingement surface materials (bubble formation and departure), d) influence of non-condensable and liquid-dissolved gases on nucleation sites activity, e) degree of subcooling, f) temperature excursions (overshoot) at incipience, and g) nucleation onset and hysteresis, as affected by the heating method, have all been investigated [10]. Knowledge on spray impingement heat transfer, on the other hand, present is still maturing. Most of the investigations are pushed by well-defined technological demands [1,2,4,5].

Figure 1 schematically depicts the geometry of square spray arrays. Parameters include pitch, D, the distance separating neighboring nozzles, and height, H, from nozzles discharge orifices to impingement surface. Nozzles breakup coolant into a full-cone shaped mist of angle θ. Droplets, formed by an isolated nozzle, impact the impingement surface over a disk-shaped region. Nozzles of an array may be arranged in a staggered or in an in-line (square) pattern. Staggered arrays can be thought as dividing the impingement surface in a number of adjacent, hexagonal-shaped, modules of symmetry. The centre of each module would lie exactly below its corresponding nozzle. Analog modules of symmetry, of an in-line array, would be square-shaped.

Three different possibilities for direct impact disks patterns, as coolant impinges on an indefinitely large square array of sprays, are represented in Fig. 1. For a given spray cone angle, θ, pitch, D, and nozzles-to-impingement surface distance, H, the disk-shaped loci where coolant from adjacent nozzles impact may overlap or not. The pattern of a square array, where neighboring spray cones do not overlap, is shown in the upper part of Fig. 1. Here, among the multiple possibilities for arrays subdivision in distinct modules of symmetry, two square-shaped modules are highlighted. Their edges are located immediately below four spray nozzles. One contains a fifth nozzle, right at the centre of the symmetry module. The other does not. The lower part of Fig. 1 depicts two additional possibilities for

impingement patterns over such modules of symmetry. Adjoining impact disks may slightly (lower right-hand side) or highly (lower left-hand side) overlap.
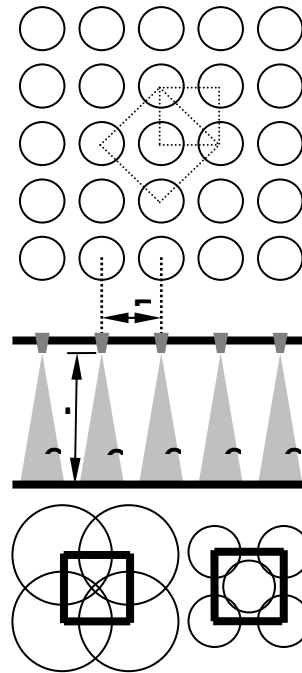
Figure 1: Geometry of square arrays of impinging sprays.

The occurrence of the varying impingement patterns, as referred above (Fig. 1), is associated to the ratio, ψ, of spray cone base radius, *H tan(θ/2)*, and nozzle-to-nozzle pitch, D:

$$\psi = \frac{H \tan\left(\frac{\theta}{2}\right)}{D} \qquad (1)$$

Such aspect ratio was successfully employed for correlating the single phase heat transfer data of in-line spray arrays [8]. Equation 2, below, reproduce all the 230 original experimental points, employed in its deviation, with a mean absolute error of 6.29 %.

$$Nu = 5.51e^{-1/31.4\psi} \, \mathrm{Re}^{0.773} \, \mathrm{Pr}^{0.609} \qquad (2)$$

The adoption of D-based Nusselt and Reynolds numbers led to a correlation where the classical $Nu \propto Re^{0.8}$ proportionality, typical of turbulent flows, was verified. All the coefficients of Eq. 2 were simultaneously obtained of a least squares fit. Original data spanned though the $0.1 < \psi < 0.9$, $50 < Re < 900$ and $2.7 < Pr < 5.6$ ranges. All of the coolant transport properties, in this correlation, are to be evaluated at the film temperature, averaged between wall and liquid temperatures. Spray-related parameters, such as calculated droplet Sauter mean diameter, nozzles discharge velocity and coolant surface tension were observed to have no measurable effect on the single phase heat transfer [8].

This work further contributes to the understanding of heat transfer in square spray arrays by presenting experimental data on the nucleate boiling heat transfer regime. Multiple spray nozzles were positioned above a square, upward-facing, 100 cm[2] copper heat-dissipating surface. Array geometry were varied by adjusting nozzle-to-nozzle (70.7 and 100 mm), nozzle-to-impingement surface distances (20, 50, 80, 100 and 145 mm). Full-cone spray angle was observed in the $40° < \theta < 60°$ range. Highly subcooled water ($30 < T_{SAT}–T_L < 75$ °C) was the convective media. The experimental construction allowed for good drainage of spent coolant and unrestricted air entrainment to spray cones.

2. The experiments

Figure 2 presents a schematic representation of the experimental apparatus. Ordinary mains water was collected into a small, constant level, tank. From there water flowed through a sharp edge orifice plate meter, placed upstream of a multistage, high pressure, centrifugal pump. Water was filtered before distribution to the spray nozzles, mounted on the test chamber upper end. A manual by-pass valve, connecting pump suction and discharge lines, was used for adjusting water flow rate to the test section. The flow meter was mounted on the pump suction line in order to avoid pulverization

pressure level on the instrument (and the associated leakage risk). The tank, isolating the apparatus hydraulic system from uncontrolled pressure fluctuations on the laboratory water supply line, assured steady flow thought pulverization nozzles.
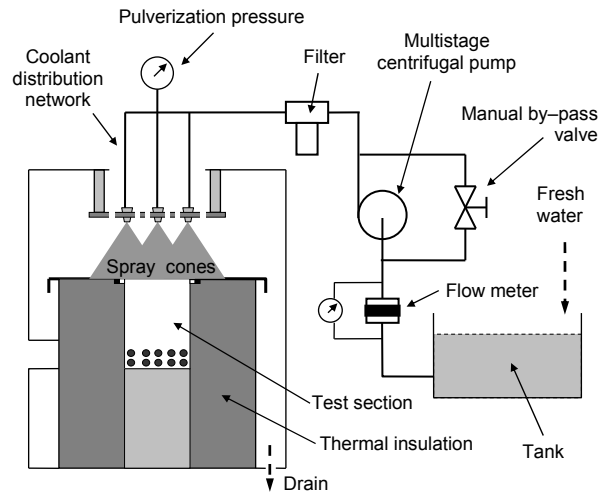
Figure 2: Schematics of experimental setup.

Total water flow rate was varied over a broad range (40 – 650 kg/h). Three sharp edge orifice plates, of varying flow passage diameters, were built to work, one at a time, in association with a single FP2000 Series SENSOTEC differential pressure transducer (1 psid, 0.1% FS uncertainty). The sharp edge orifice plates were designed to cover, when installed in the flow meter, the whole flow range in three successive, somewhat overlapping, intervals. For a given plate (flow interval) transducer readings were, typically, not smaller than 15% of the instrument full scale. Avoidance of low differential pressure readings, of high relative uncertainty, contributed to diminish uncertainty propagation into the coolant mass flow rate calculation. Single sample uncertainty analysis [11] indicates that water flow error was, typically, smaller than 3 %. Uncertainties on discharge coefficients, as observed in meters calibration process (ratio of weight of water collected in a separate small-volume tank by stopwatch-monitored time), accounted for most of this value.

Pressurized water was filtered for particulate removal, as coolant suspensions could erode or clog pulverization tips flow passages. A damaged nozzle, not necessarily displaying modified flow capacity, invariably has the pulverization pattern compromised. Droplet and cone formation, as well as coolant distribution over the impingement surface, may suffer from eroded or partially clogged spray nozzles.

A 10 bar pressure transducer (SENSOTEC FP2000 Series, 150 psig, also of 0.1% FS uncertainty) was used to monitor pulverization pressure. The sensor was installed downstream the filter, where fluid flow was split among the various branches that distributed pressurized coolant to array nozzles. Flexible hoses were used for supplying water to the multiple spray cones. Pressure drop along those hoses was negligible when compared to measured pulverization pressure. K-type thermocouples were installed just upstream from where every spray nozzle connected to the coolant distribution network. Probes calibration indicates 0.3 ºC uncertainties in their readings. Sprayed coolant temperature, T_L, was taken as the average of those measured in all nozzles. Instrumentation signals were monitored and registered by a digital data acquisition system.

The test chamber, part of the experimental setup specially built for this investigation, is illustrated on the left-side of Fig. 2. A number of spray nozzles, attached to a common support plate, could be positioned at adjustable distances from a 100 x 100 mm square heat-dissipating copper surface. This metallic part was mounted inside a glass-wool, thermally-insulated, polypropylene box. Numerical simulations [6] of heat diffusion in the setup, obtained during test chamber design phase, revealed that, fundamentally, all of the heat would be dissipated through the surface exposed to spray impingement. An outer Plexiglas box, to which a nozzle support plate was mounted, allowed for observation of the impingement pattern and spent water collection. A Teflon collar, press-fit to the copper test section (close to its impingement-exposed surface), prevented water leakage to the interior of the polypropylene box. A 1.0 mm thick stainless steel cap, screwed to the Teflon collar, closed the heater box upper end.

Runs were, in resemblance to the modules of symmetry sketched in the lower part of Fig. 1, conducted with four or five operational spray nozzles. During the four-nozzle runs, sprays were positioned above the corners of the heat dissipating surface. This arrangement was intended to reproduce the hydrodynamic and thermal conditions that would be verified in symmetry modules of indefinitely larger square arrays (of pitch equal to 100 mm). The fifth nozzle was positioned exactly above the centre of the heat-dissipating surface. Runs that had this fifth nozzle operational intended to reproduce arrays of D equal to 70.7 mm.

The test section basically consisted of a 100 x 100 x 140 mm copper block, machined for exact dimensions, electrical cartridge heaters assembly and thermocouple instrumentation (Fig. 3). Ten high-temperature cartridge heaters were press fit into holes drilled at the bottom of this test section. The heaters were 100 mm (4") long and, together, could dissipate up to 10 kW. Heat conduction through the metallic part was, from the heaters region to the impingement surface, fundamentally one-dimensional. This resulted from test section insulation and copper block dimensions. Cartridges were placed, and operated, seeking an as uniform as possible heat-dissipation in the test section base. This assisted in obtaining one-dimensional heat diffusion already at short distances from where heaters were mounted. The heat load of one of the two five-heater rows (the one close to test section lower end, Fig. 2) was manually set by a thyristor-based power supply. The other row was simply operated on or off. When setup power was to be adjusted in a low load condition, this second row was kept off. Electrical power, dissipated in the first row, could be continuously adjusted up to maximum of the heaters power. Testing at increased heat flux conditions was performed with the second row of heaters operational. F̶ ̶tal heat load was, in those situations, also accomplished t̶ ̶irst row power. The five heaters of a given row alwa̶ ̶the same power. Heaters assembly holes are depicted on t̶ ̶ ̶ ̶ ̶ ̶ ̶ ̶ ̶ ̶ ̶ ̶ ̶ ̶ ̶ ̶3.
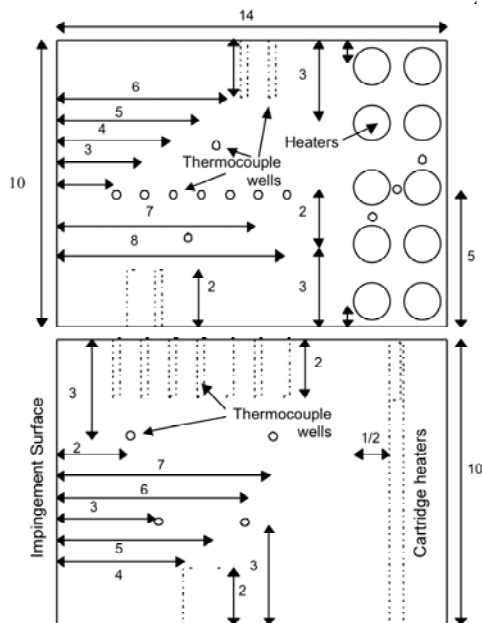
Figure 3: Machined test section dimensions (in mm).

A total of sixteen K-type thermocouples monitored test section temperature distribution. Thermocouples were placed in 1.0 mm diameter, 20 mm depth, wells (Fig. 3). Thirteen of those probes monitored temperature distribution along the main heat diffusion direction. Thermocouples wires were encased in stainless steel shields and insulated by powdered magnesium oxide. Probes calibration indicates an uncertainty of 0.3 ºC on temperature readings. Three of the thermocouples were, for safety reasons, positioned close to the cartridge heaters. The maximum allowable temperature for those probes was set, in an apparatus protection device, at 600 ºC. Heaters power was automatically interrupted in case of high temperature detection. Test chamber protection against unacceptably high temperatures was, thus, assured.

Thermocouple wells (Fig. 3) were distributed along the test section in two distinct patters. Seven of probes were placed in-line, along the middle of one of the 100 x 140 mm test section surfaces. They monitored temperatures of distinct planes, normal to main heat flux, at every 10 mm. The other six thermocouples were installed in planes 5 mm apart of those seven, i.e., overlapping, the ones monitored by the in-line probes row. Wells for these other six probes were drilled according to a spirally-shaped pattern (two probes at each of the three remaining 100 x 140 mm surfaces). The 20 mm wells did not reach test section centre line. The resulting thermocouples location allowed for both: i) measuring, and confirming, the one-dimensional temperature distribution along the main heat diffusion direction, and, ii) inferring how well temperatures distribute in a given cross-section. If one-dimensional heat diffusion was really verified, planes normal to the heat flux should to be isothermal and all thirteen thermocouple readings should align in a same straight line (uniform thermal conductivity), in spite of their varying position in different planes. Figure 4 presents typical temperature distributions, taken during the experimental runs. Plots indicate attained success in establishing, along a significant part of the 140 mm test section, the pursued one-dimensional heat conduction. Error bars, for uncertainties of Fig. 4 data, were not presented, as they would result smaller than plot symbols.

Least-square curve fitting straight lines through measured temperature distributions allowed for both determining impingement surface temperature and temperature gradient induced heat flux. The impingement surface temperature, T_W, was considered to be that resulting from the extrapolation of the curve-fitted linear distribution. The average heat flux, dissipated over the impingement surface, was taken as the product of the curve-fit temperature gradient by the test

section thermal conductivity. Copper conductivity was evaluated at the mean test section temperature. Heat flux uncertainties were, for data collected in the nucleate boiling regime, estimated to be within 1.3 – 1.7 % of measurements. Uncertainties of the average heat-dissipating surface temperature are, typically, in the 0.6 – 1.2 ºC range.
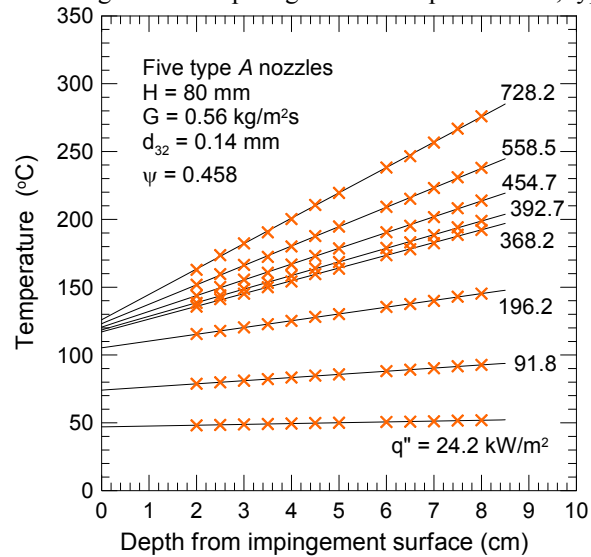
Figure 4: Typical temperature distributions within the test section.

Figure 5: Spray nozzles – Type *A* (top), *B* (centre) and *C* (bottom).

Testing routine involved the application of eight, always progressively increasing, heat fluxes. Those spanned, approximately, the 20 – 800 kW/m² range. Cartridge heaters power was applied after the number of sprays, nozzle type, H, D and pulverization pressure were set. The apparatus was considered to be operating in steady-state conditions when temperature readings, along the test section, did not oscillate more than 0.3 ºC over five minutes intervals. About 30 min. elapsed, after power adjustments, until a novel stable operating condition occurred.

Three different types of commercially available full-cone spray nozzles were employed in the present investigation. Figure 5 display both fully assembled nozzles and views of corresponding pulverization tips. Coolant atomization results of high liquid discharge velocity and swirl. Those, in their turn, are obtained during operation of spray nozzles at significant pressure differentials. Pulverization tips geometry promote not only coolant jet breakup but, also, the full-cone shaped droplet dispersion. Because of their construction, liquid droplets, formed just after coolant ejection, distribute evenly along the cone-shaped mist. The three different constructions, referred to as models *A*, *B*, and *C*, had discharge orifice diameters of, respectively, 0.53, 0.65 and 1.19 mm. All nozzles samples were factory-tested for assured droplet formation and dispersion (cone built-up). Table I presents nozzles nominal flow capacities. Because their distinct construction, the area-averaged impinging coolant mass flux could, during the experiments, be adjusted over a relatively broad range (0.3 – 7.2 kg/m²s).

Pressure spray nozzles can be built to disperse droplets in a variety of patterns, other than the conical-shaped. According to the pulverization tip construction, nozzles can create mists that would impact a heat-dissipating surface in: i) elliptical-shaped, ii) ring-shaped (hollow cones), or, iii) square-shaped (pyramidal cones) areas [12]. Full-cone nozzles, of special construction, can be used to disperse coolant over wide (~110-130º) or narrow (~10-20º) angle cones. Those alternative constructions are usually not mentioned in spray impingement heat transfer literature. Despite of a few exceptions, that came to author's knowledge [13], most of the recent spray impingement data were obtained from tests of standard full-cone angles (~40-70º) nozzles.

A total of 149 runs were conducted, under nucleate boiling conditions, on arrays of varying geometry, pulverization nozzle type, flow rate, heat fluxes and subcooling. Further details on both setup construction and experimental procedure can be found elsewhere [6-8].

2.1. Data reduction

The nucleate boiling of subcooled liquids, both in internal (pipe) flow [14] and other convective arrangements [5], is often expressed by:

$$q'' = q''_{SP} + q''_{NB}$$ (3)

Here the wall heat flux, q", is considered as composed of two independent, though simultaneous, single-phase, q"$_{SP}$, and boiling, q"$_{NB}$, contributions to the total heat transfer. In the case of pipe flow boiling [14], known correlations such as Dittus-Boelter [15] can be used for estimating the single-phase component.

In the present work Eq. 2 was used for determining the q"$_{SP}$ term [8]. Substituting Eq. 2 in 3 results in:

$$q''_{NB} = q'' - \frac{k_f}{D}\left[5.51e^{-1/31.4\psi}\left(\frac{GD}{\mu_f}\right)^{0.773}\left(\frac{\mu_f c_{Pf}}{k_f}\right)^{0.609}\right](T_W - T_L)$$ (4)

The phase change contribution, q"$_{NB}$, to the total heat flux, q", is traditionally observed to depend on the wall temperature excess, $T_W–T_{SAT}$. Surface finish and surface-fluid combination are also parameters to be considered. Both influence not only bubble formation and departure processes but, also, the distribution and number of nucleation sites along a heat-dissipating surface. The vapor production capabilities of a surface, varying with its material, finish and fluid properties, reflect on q"$_{NB}$. For practical purposes the resulting effect of those parameters, all acting simultaneously on a specific situation, must be determined experimentally.

As ordinary mains water was used as coolant, fouling was observed to build up over the impingement surface. Through visible, these deposits revealed extremely faint and had no measurable influence on the measured heat transfer characteristics of tested arrays. To guarantee constant surface conditions throughout the experiments, the impingement surface was, on a daily basis, re-polished to a mirror-like aspect with no. 600 emery cloth.

Atmospheric pressure readings were performed using a SENSOTEC FP2000 Series barometer (26-32" Hg, 0.1 % FS uncertainty). Records indicate that, during experimental runs, atmospheric pressure variations were restricted to the 100.5-101.5 kPa range. Water saturation temperature, at such pressure level, fundamentally equals 100 ºC. Uncertainty of T_{SAT} was, based on observed fluctuations of barometric pressure, estimated to be within ±0.5 ºC.

Spray impingement literature [1,3] frequently refers to performance parameters such as cooling effectiveness (Eq. 5) and efficiency (Eq. 6) when presenting boiling heat transfer data. They are defined as follows:

$$\varepsilon = \frac{q''}{G}$$ (5)

$$\eta = \frac{q''}{G\left[c_{Pf}\left(T_{SAT} - T_L\right) + h_{fg}\right]}$$ (6)

Cooling effectiveness indicates the amount of heat absorbed by a given mass of sprayed coolant (some authors refer to volume [4]). Cooling efficiency indicates the ratio of the actual heat flux to the one that, if transferred to coolant, would lead to its complete evaporation.

Water vapor formed on the impingement surface invariably closely interacts with incoming liquid droplets. Because of that, vapor, that leaves impingement region, can, in principle, be considered as saturated. Some authors [16] suggest that, for completeness, a superheat term, which would account for possible vapor heating up to T_W, should be considered.

The Weber number, parameter associated to deformation patterns and heat transfer of impacting droplets [1-3], is given by:

$$We = \frac{\rho_f v^2 d_{32}}{\sigma_f}$$ (7)

The characteristic velocity employed in Eq. 7, v, was taken as the ratio between measured volumetric flow rate and spray nozzles total discharge area. Droplet Sauter mean diameter, d_{32}, was calculated using the correlation proposed by Estes and Mudawar [17]. These authors derived such expression from experimental data on atomization tips of construction and operating conditions resembling those of nozzles *A*, *B* and *C* (same nozzle manufacturer and of similar types).

3. Results and discussion

Figure 6 plots representative boiling curves obtained from tests on arrays of type *A* nozzles. Measured heat flux, q", is presented as a function of impingement surface temperature, T_W, at typical operating conditions. For a given geometric aspect-ratio, ψ, and average impingement coolant flux, G, a fairly linear relationship between q" and T_W is observed (at wall temperatures below 100 ºC). In this range, as $T_W < T_{SAT}$, only single-phase heat transfer occurs. The different slopes of the single-phase plots result from distinct heat transfer coefficients, h$_{SP}$, which vary according to array geometry and impinging coolant flux. Augmented h$_{SP}$ reflects in curves of steeper slopes. Comparing data of

arrays operating on G of 0.56 kg/m²s, for example, the one of ψ equal to 0.286 displays an increased single-phase heat transfer coefficient, when confronted to the other, of reduced ψ (0.115). The effect of ψ on h_{SP} is relatively modest when compared to that of G. The array with $G=1.28$ kg/m²s and $\psi=0.407$ displays remarkably increased h_{SP} when compared to the one of 0.28 kg/m²s. This results even with the aspect-ratio, ψ, of latter (0.587) being superior to that of the array operating on 1.28 kg/m²s.

Heat fluxes significantly augment with T_W as impingement surface surpass 100 ºC and its excess temperature, T_W-T_{SAT}, is further increased. Also plotted in Figure 6 is the experimentally obtained expression for the phase change contribution to the total heat flux, q"$_{NB}$ (Eq. 8). For now it's worth noting that boiling curves of arrays with comparatively reduced h_{SP} tend to merge such q"$_{NB}$ curve at, also, diminished wall excess temperatures. As h_{SP} increases boiling curves shift upwards. In any case those, at a sufficiently high T_W-T_{SAT}, are also expected to merge q"$_{NB}$. Curves of different arrays, once approximating such boiling curve, are all expected to closely follow q"$_{NB}$.
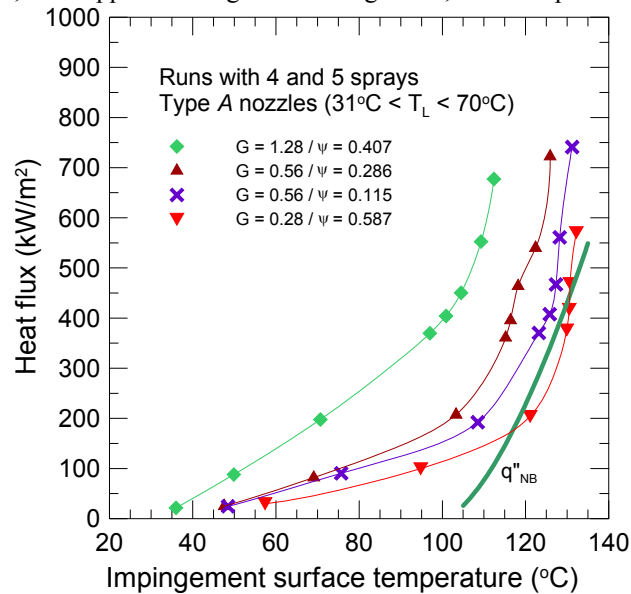
Figure 6: Typical boiling curves of type *A* nozzle arrays.

Figure 7 (a) presents some representative boiling curves for arrays of *B* type nozzles. Changes to arrays parameters, such as G and ψ, have effects similar to those just described when discussing Fig. 6. Because of the increased flow capacity of *B* type nozzles (i.e., also increased h_{SP}), boiling curves of Fig. 7 (a) typically lie above those presented in Fig. 6.

An example assists in illustrating that the total heat flux, q", can be considered as composed of simultaneous single-phase, q"$_{SP}$, and nucleate boiling, q"$_{NB}$, heat transfer contributions. Attention is directed to one particular boiling curve, presented in Fig. 7 (a), relative to an array of G and ψ equal to 0.56 kg/m²s and 0.202, respectively. Its specific single-phase linear relationship, q_{SP}"(T_W), as determined from Eq. 2, was extrapolated for the $T_W > T_{SAT}$ region. Evaluating q"$_{SP}$ and q"$_{NB}$ curves at T_W equal to 127 ºC, temperature for which q" data is available, it is observed that the single-phase and boiling contributions equal, respectively, 213.6 and 365.2 kW/m². The $q"_{SP}+q"_{NB}$ heat flux (578.9 kW/m²) results only 3 % higher than measured q" (561.6 kW/m²). As boiling curves result from contributions of both q"$_{SP}$ and q"$_{NB}$, they: i) approach the linear single-phase relationship when q"$_{SP}$ is significantly larger than q"$_{NB}$, and, ii) merge on the q"$_{NB}$ boiling curve in arrays of comparatively low h_{SP} and (or) high wall excess temperature, T_W-T_{SAT}.

Some representative boiling curves for *C* type nozzle arrays are presented in Figure 7 (b). Because of the high single-phase heat transfer coefficients verified in those arrays, most of the heat flux was, systematically, absorbed by the q"$_{SP}$ component. Comparing Fig. 7 (b) data to that of other nozzle types (Figs. 6-7), comparatively modest wall excess temperatures (typically below 20 ºC) are verified. Many runs resulted limited to the single-phase regime. This was the case of the array with G equal to 7.16 kg/m²s.

Sprayed coolant temperature, although continuously monitored, was not controlled. Pumping power, dissipated in the by-pass (Fig. 2), and moisture condensation over the liquid distribution network resulted in T_L variations. Sprayed water temperature stabilized, according specific setup operating conditions, on distinct values. Those were, typically, in the 25 – 70 ºC range. Variations on both T_W and T_L affect liquid film temperature, i.e., coolant transport properties (k_f, Pr_f and μ_f). Those, by their turn, also influence h_{SP} (Eq. 2). Those impact Figs. 6-8 by: i) distorting single-phase regime q"$_{SP}$(T_W) linearity, and, ii) shifting curves, as both h_{SP} and T_L vary ($q"_{SP}=h_{SP}T_W-h_{SP}T_L$). Error bars, if included in Figs. 6-8, would result within the size of plot symbols. Heat flux and T_W uncertainties are estimated lower than, respectively, 1.7% and 1.2 ºC.
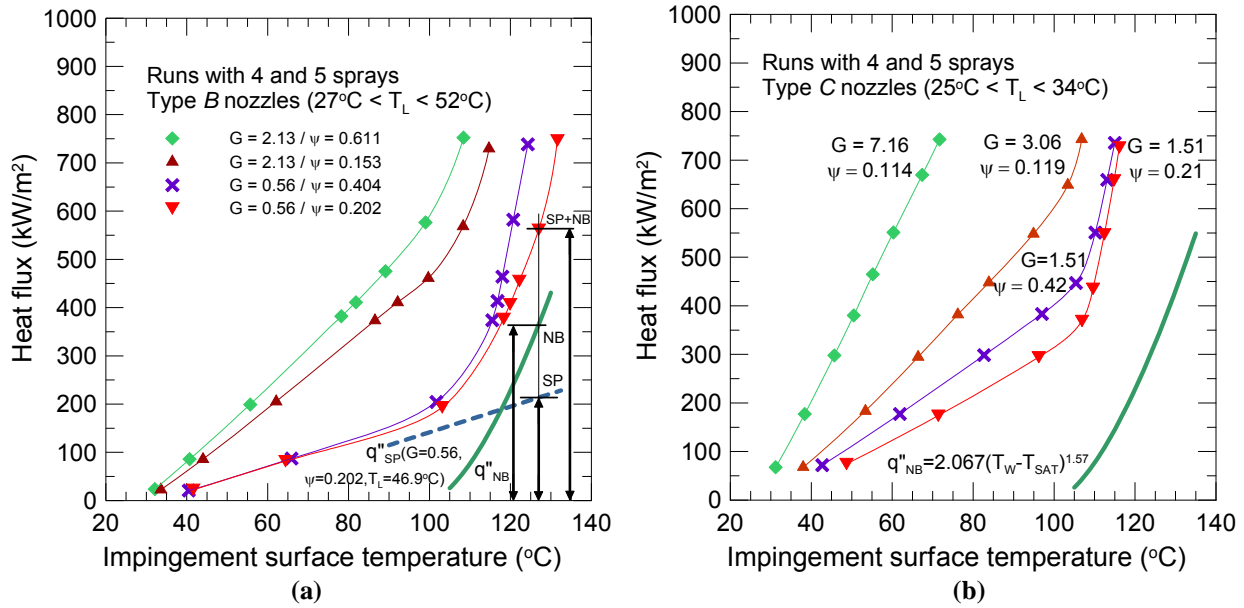
Figure 7: **(a)** Typical boiling curves of type *B* nozzle arrays and **(b)** Typical boiling curves of type *C* nozzle arrays.

The q''_{SP} plot in Fig. 7 indicates Eq. 2 predictions for the specific G, ψ and T_L of the experimental point considered when discussing the $q''_{SP}+q''_{NB}$ additivity. It can be noticed that, when this particular expression is extrapolated to the $T_W < T_{SAT}$ region, it does not overlap corresponding array single-phase data. This would be the case if both h_{SP} and T_L were constant. Variations on T_L are those that, primarily, do not allow for the simple extrapolation of single-phase results, into the $T_W > T_{SAT}$ region, for predicting q''_{SP}. Coolant temperature was observe to increasingly augment, while sampling such detailed discussed boiling curve of Fig. 7 (a), from 33.1 to 51.2 ºC. For the specific point considered in the $q''_{SP}+q''_{NB}$ additivity example, T_L equals 46.9 ºC.

Phase change contributions to the total heat flux were obtained (Eq. 4) by subtracting q''_{SP} estimates (Eq. 2) from measured q'' (Eq. 3). Figure 8 displays the dependence of $q''-q''_{SP}$ on wall excess temperature, T_W-T_{SAT}. Horizontal error bars indicate typical uncertainties, usually in the 1.0 – 1.5 K range, for T_W-T_{SAT}. Experimental points where T_W is relatively close to T_{SAT} are those where wall excess temperatures uncertainties are of the order of T_W-T_{SAT}. Individual uncertainties of both T_W and T_{SAT} display diminishing relevance to wall excess temperature uncertainties as T_W progressively increases. Vertical error bars result from raw data error propagation through Eq. 4. Operating conditions where q''_{SP} nearly equals q'' (low wall T_W-T_{SAT}) are, also, those of increased q''_{NB} uncertainties. As the $q''-q''_{SP}$ difference increases its uncertainty diminishes. As the graph would be overcrowded with error bars, if depicted for all data, decision was taken on plotting uncertainties only for some of the points. Those reflect typical error intervals, also verified in the rest of the data.
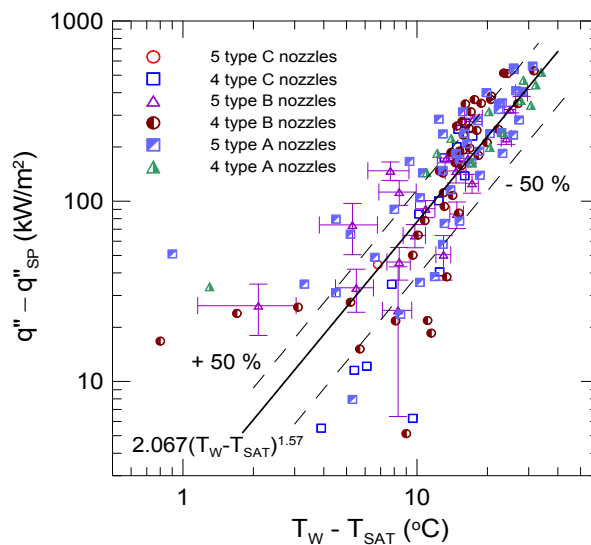
Figure 8: Phase change contribution to total heat flux.

The nucleate boiling contribution to total heat flux was correlated by:

$$q''_{NB} = 2067(T_W - T_{SAT})^{1.57} \qquad\qquad (8)$$

This expression reproduces phase change contributions to total wall heat flux within, approximately, ± 50%. Data scattering, although significant at lower wall excess temperatures (where uncertainties are significant), is fairly symmetrical around Eq. 8 and does not suggest that its form should be considered inappropriate. In spite of varying array geometry, flow rate and spray nozzle type (of distinct atomization characteristics), q"$_{NB}$ appears to be a function of T_W-T_{SAT} only. This q"$_{NB}$ expression is plotted in Figs. 6-7.

Numeric values of Eq. 8 coefficients are associated to the specific conditions of the experiments. Its use should, therefore, remain restricted for applications where water is to impinge on, if not polished, well finished copper surfaces. If spray cooling is to occur in environments where the ambient absolute pressure significantly differs from 1 bar, where coolant properties of relevance to q"$_{NB}$ (specifically vapor density) vary, predictions of Eq. 8 may deviate. This would be the case if the surface to be cooled was, for example, in the interior of a pressurized vessel.

Comparisons of Eq. 3 predictions, to measured q", are plotted in Figure 9 (a). Original data is reproduced with an average mean error of 10.6 %. The boiling component correlation (Eq. 8), q"$_{NB}$, in spite of reproducing raw data with significant scatter at low T_W-T_{SAT} (Fig. 8), accounts for a low percentage of $q''_{SP}+q''_{NB}$ when T_W is close to T_{SAT}. As a result $q''_{SP}+q''_{NB}$ uncertainties, no matter what T_W-T_{SAT} value, lie in the 1.1 – 4.7 % range.

Figure 9 (b) illustrates the insensitiveness of heat transfer to droplet-related parameters. The ratio of measured heat flux, q", to Eq. 3 predictions is plotted against the Weber number (Eq. 7). If nozzles discharge velocity, calculated d$_{32}$ or coolant surface tension were of considerable influence to the single-phase or boiling contributions to total heat transfer the $q''/q''_{SP}+q''_{NB}$ ratio would be expected to, systematically, vary with We. No noticeable trend of $q''/q''_{SP}+q''_{NB}$ on We can be inferred from Fig. 9 (b) as data simply scatter, within the ± 30 % range (also presented in Fig. 9 (a)), around 1.0.

The insensitiveness of both q"$_{SP}$ and q"$_{NB}$ to atomization parameters, such as calculated droplet Sauter mean diameter [17] and nozzles velocity, indicate that mechanisms of relevance to heat transfer remain, in the single-phase and nucleated boiling regimes, limited to the coolant film that wets the impingement surface. The use of droplet-related parameters, in correlating q"$_{SP}$ and q"$_{NB}$, may prove not fully appropriate in scaling relevant phenomena. As in the fully developed nucleate boiling of other impingement arrangements [18-20], spray array geometry and flow rate also appear to have little effect on the $q''_{NB} x (T_W$-$T_{SAT})$ interdependence. In the case of jet impingement boiling hydrodynamic-related parameters, such as jet geometry and flow rate, determine at witch specific critical (or maximum) heat flux boiling curves shift from the fully developed to the transition boiling regimes. Jet velocity and impingement geometry affect the way fresh coolant, displacing spent vapor, reaches a heat-dissipating surface [10].
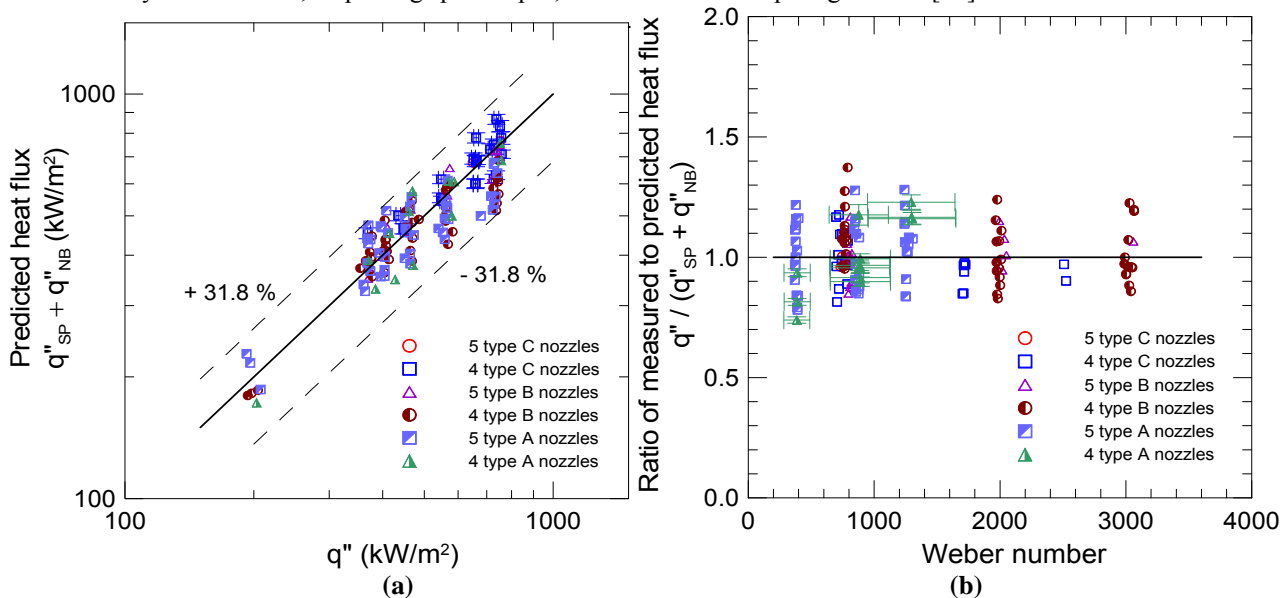
Figure 9: **(a)** Comparison between Eq. 3 predictions and measured heat flux and **(b)** Heat transfer insensitiveness to Weber number.

Cooling efficiency (or effectiveness) is usually associated [3-4], at CHF conditions of impinging sprays, to droplet-dependent parameters (We). This suggests that, in the vicinity of q"$_{CHF}$, where boiling shifts from the nucleate to the transition regimes, the liquid film wetting impingement surface probably results thinned or, even possibly, non-existent over part of the impingement surface. This condition would open room for direct droplet impact over a bare, dry, heat-dissipating impingement surface. Investigations on the We-dependant heat transfer and deformation patterns (including possible rebound) of isolated droplets impacting heated, dry surfaces, proved capable of predicting spray impingement heat transfer in the transition and film boiling regimes [21-23].

Figures 10 (a) and (b) illustrate, respectively, cooling effectiveness and efficiency variations, of all tested arrays, to wall excess temperature. Both ε and η continually increase, for a given array geometry and flow rate, with applied heat flux. Maximum ε and η would be verified at CHF. Different sprays or spray arrays performance (ε and η) can only be fairly compared at this limiting condition, i.e., using ε_{CHF} and η_{CHF}. In any, case Figs. 10 (a) and (b) present representative data and, eventually, may show helpful when a approximate guidance, on what to expect from the heat transfer to water spray arrays, is needed. Non-CHF cooling effectiveness and efficiencies of up to, respectively, 2,000 kJ/kg and 83 % were observed. Those refer to the experimental point, plotted in Fig. 6, for a type *A* nozzle array operating on G, ψ and q" of, respectively, 0.28 kg/m²s, 0.587 and 571 kW/m².
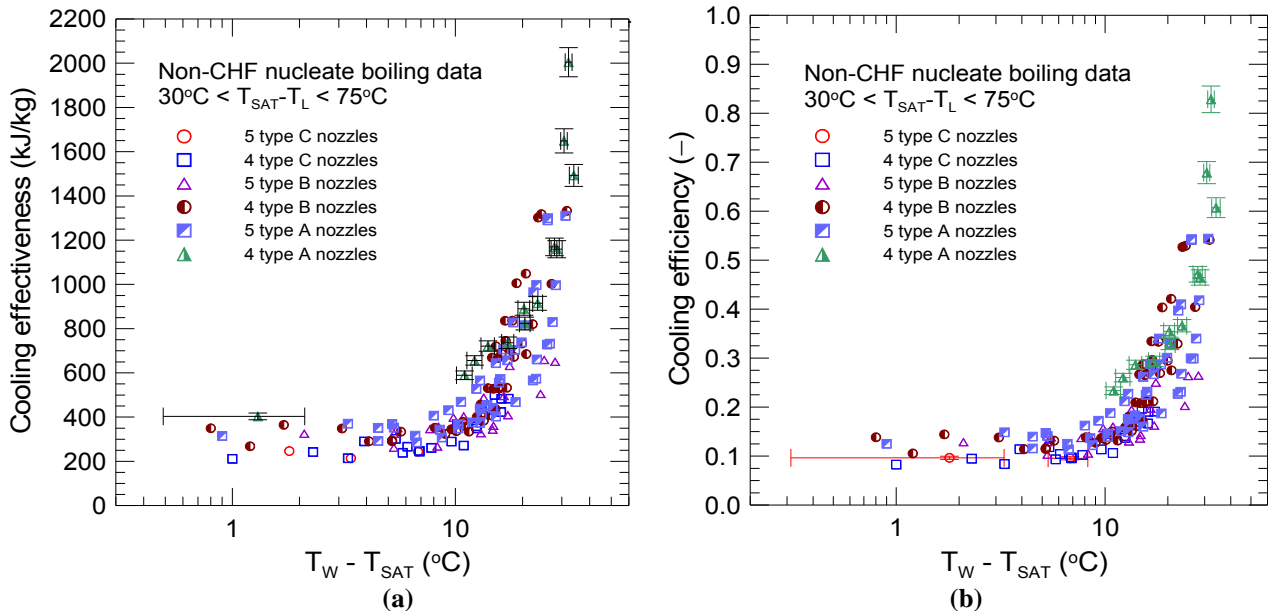
Figure 10: **(a)** Non-CHF cooling effectiveness variation with excess wall temperature and (b) Non-CHF cooling efficiency variation with excess wall temperature.

Following the condition where η of 83% was observed, power was readjusted to an increased heat flux (~725 kW/m²). Test section temperature distribution, at this new operating condition, did not asymptote to a novel, somewhat increased (but close to that verified at 571 kW/m²), linear temperature distribution. Temperatures kept, though slowly, progressively increasing. This indicates that CHF occurred, at the specific conditions of such spray array, at q" somewhere between 570 and 730 kW/m². A non-CHF operating condition, if attained at such increased heat flux, would correspond to a cooling efficiency of, approximately, 100%.

Test section was allowed to heat until temperatures around 300 ºC were verified at readings from the thermocouple close to the Teflon collar (also the one closest to impingement surface, Fig. 3). At this point, the heaters power was cut. The setup, during this transient operation, certainly experienced the transition boiling regime. Droplets were observed to strike and rebound from the high temperature impingement surface. Nucleate boiling was reestablished when the test section, still being sprayed and cooled, once again crossed the CHF condition. A sudden, noisy and visible rewetting of the impingement surface was accompanied by a massive vapor formation (when compared to that of the transition boiling regime). Apart of this brief description of observed setup transient operation, no data reduction was attempted on test section transient temperature readings. This was the case for some literature-reported investigations [24,25].

This work, though focusing on the (steady-state) nucleate boiling of spray arrays, did not attempt correlating associated CHF conditions. Little data was gathered on CHF as, because of setup increased thermal inertia, q"CHF was found difficult precise. Alternative experimental constructions, of reduced thermal inertia and where the burn out of (disposable) heat-dissipating surfaces is actually intended, may prove best suited for the accurate quantification of q"CHF. Because of the varying impact patterns that may result of array geometry (Fig. 1), it is reasonable to assume that, as in the case of other impingement arrangements [24,25], a given heat-dissipating surface may, eventually, experience all the distinct boiling regimes at a time. Jet impingement literature reports that, according to surface temperature, jet geometry, velocity and subcooling all single-phase, nucleate, transition and film boiling regimes may all occur simultaneously at different streamwise locations on target surfaces [10]. Measurement of local heat transfer in impinging spray arrays, not performed in the present work, may bring light to the matter.

4. Concluding remarks

The nucleate boiling of subcooled water, under 100 cm² square arrays of impinging sprays, was experimentally investigated. Three types of commercially-available full-cone pressure nozzles, of varying flow capabilities, allowed for

runs where the average impinging coolant mass flux spanned broad ranges (0.3 – 7.2 kg/m²s). Array geometry was varied adjusting nozzle-to-nozzle (70.7 and 100 mm) and nozzle-to-impingement surface (20, 50, 80, 100 and 145 mm) distances. Experimental construction allowed for good drainage of spent coolant and unrestricted air entrainment to spray cones. The average heat flux through the heated, upward-facing, copper test section was found to equal the sum of single-phase, q''_{SP}, and boiling, q''_{NB}, heat flux components:

$$q'' = q''_{SP} + q''_{NB} \tag{3}$$

Contributions to the prediction of the total heat flux are re-written below:

$$q''_{NB} = 2067(T_W - T_{SAT})^{1.57} \tag{8}$$

$$\frac{q''_{SP}}{T_W - T_L} \frac{D}{k_f} = 5.51 e^{-1/31.4\psi} \left(\frac{GD}{\mu_f}\right)^{0.773} \left(\frac{\mu_f c_{Pf}}{k_f}\right)^{0.609} \tag{2}$$

The $q''_{SP} + q''_{NB}$ expression reproduces all the 149 original experimental points with a mean absolute error of 10.6 %.

Transport properties in Eq. 2, derived from experimental data in the $0.1 < \psi < 0.9$, $50 < Re < 900$ and $2.7 < Pr < 5.6$ ranges [8], are to be evaluated at the film temperature (average between T_W and T_L). Array geometry is described by the aspect-ratio ψ:

$$\psi = \frac{H \tan\left(\theta/2\right)}{D} \tag{1}$$

Numeric values for the coefficients of Eq. 8 are associated to the specific conditions of the experiments. Its use should, therefore, remain restricted for applications where water is to impinge on well finished, if not polished, copper surfaces.

The insensitiveness of both q''_{SP} and q''_{NB} to atomization parameters, such as calculated droplet d_{32} and nozzle discharge velocities, indicates that mechanisms of relevance to heat transfer may, in the single-phase and nucleated boiling regimes, be those within the coolant film that wets the impingement surface. The use of droplet-related parameters, in correlating such data, may prove not fully appropriate in scaling relevant phenomena. As in the case of other impingement arrangements [18-20], spray array geometry and flow rate also appear to have little effect on q''_{NB}.

Non-CHF cooling effectiveness and efficiencies of up to, respectively, 2,000 kJ/kg and 83 % were observed. In those conditions, where most of the impinging coolant evaporates, the liquid film wetting impingement surface probably results thinned or, even possibly, non-existent over part of the impingement surface. This would open room for direct droplet impact over a bare, dry, heat dissipating surface.

ACKNOWLEDGMENTS

REFERENCES

D.D. Hall, I. Mudawar, Optimization of quench history of aluminum parts for superior mechanical properties, Int. J. Heat Mass Transfer 39 (1996) 81-95.

D.D.Hall, I. Mudawar, Experimental and numerical study of quenching complex – shaped metallic alloys with multiple, overlapping sprays, Int. J. Heat Mass Transfer 38 (1995) 1201-1216.

J.R. Rybicki, I. Mudawar, Single-phase and two-phase cooling characteristics of upward-facing and downward-facing sprays, Int. J. Heat Mass Transfer 49 (2006) 5-16.

A.G. Pautsch, T.A. Shedd, Spray impingement cooling with single- and multiple-nozzle arrays. Part I: Heat transfer data using FC-72, Int. J. Heat Mass Transfer 48 (2005) 3167-3175.

T.A. Shedd, A.G. Pautsch, Spray impingement cooling with single- and multiple-nozzle arrays. Part II: Visualization and empirical models, Int. J. Heat Mass Transfer 48 (2005) 3176-3184.

R.H. Pereira, Resfriamento de superfícies com arranjos de jatos pulverizados ("Cooling of surfaces with spray arrays"); Master's Dissertation, Department of Mechanical Engineering, Pontifícia Universidade Católica / PUC-Rio, 1998, Rio de Janeiro, Brasil (in Portuguese).

R.H. Pereira, S.L. Braga, J.A.R. Parise, Comparing single phase heat transfer to arrays of impinging jets and sprays, Proceedings of IMECE2002, New Orleans, LA, USA, 2002, Paper IMECE2002-32531.

R.H. Pereira, S.L. Braga, J.A.R. Parise, Cooling of large surfaces with square arrays of impinging water sprays. Part I: Single phase heat transfer, Int. J. Heat Mass Transfer (submitted).

S. Freund et al., Local heat transfer coefficients in spray cooling systems measured with temperature oscillation IR thermography, Int. J. Heat Mass Transfer (2006).

D.H. Wolf, F.P. Incropera, R. Viskanta, Jet impingement boiling, Advances in Heat Transfer, 23 (1993) 1-132.

R.J. Moffat, Describing the uncertainties in experimental results, Experimental Thermal and Fluid Science 1 (1988) 3-17.

A.H. Lefebvre, Atomization and sprays, Hemisphere, New York, 1989.

A.L.N. Moreira, M.R.O. Panão, Heat transfer at multiple-intermittent impacts of a hollow cone spray, Int. J. Heat Mass Transfer 49 (2006) 4132-4151.

J.G. Collier, Convective boiling and condensation, McGraw-Hill, New York, 1981.

R.H.S. Winterton, Where did the Dittus and Boelter equation came from? Int. J. Heat Mass Transfer 41 (1998) 809-810.

T.L. Cox, S.C. Yao, Heat transfer of sprays of large water drops impacting on high temperature surfaces, J. Heat Transfer 121 (1999) 446-450.

K.A. Estes, I. Mudawar, Correlation of sauter mean diameter and critical heat flux for spray cooling of small surfaces, Int. J. Heat Mass Transfer 38 (1995) 2985-2996.

D.T. Vader, F.P. Incropera, R. Viskanta, Local convective heat transfer from a heated surface to an impinging, planar, jet of water, Int. J. Heat Mass Transfer 34 (1991) 611-623.

D.T. Vader, F.P. Incropera, R. Viskanta, Convective nucleate boiling on a heated surface cooled by an impinging, planar jet of water, ASME J. Heat Transfer 114 (1992) 152-160.

[20] D.H. Wolf, F.P. Incropera, R. Viskanta, Local jet impingement boiling heat transfer, Int. J. Heat Mass Transfer 39 (1996) 1395-1406.

J.D. Bernardin, I. Mudawar, Film boiling heat transfer of droplet streams and sprays, Int. J. Heat Mass Transfer 40 (1997) 2579-2593.

J.D. Bernardin, C.J. Stebbins, I. Mudawar, Mapping of impact and heat transfer regimes of water drops impinging on a polished surface, Int. J. Heat Mass Transfer 40 (1997) 247-267.

J.D. Bernardin, C.J. Stebbins, I. Mudawar, Effects of surface roughness on water droplet impact history and heat transfer regimes, Int. J. Heat Mass Transfer 40 (1997) 73-88.

D.E. Hall, F.P. Incropera, R. Viskanta, Jet impingement boiling from a circular free-surface jet during quenching: Part 1 – Single-phase jet, J. Heat Transfer 123 (2001) 901-910.

D.E. Hall, F.P. Incropera, R. Viskanta, Jet impingement boiling from a circular free-surface jet during quenching: Part 2 – Two-phase jet, J. Heat Transfer 123 (2001) 911-917.

RESPONSIBILITY NOTICE

The authors are the only responsible for the printed material included in this paper.